ChemComm

COMMUNICATION

View Article Online
View Journal | View Issue

Reduced TiO_2 rutile nanorods with well-defined facets and their visible-light photocatalytic activity†

Cite this: *Chem. Commun.*, 2014, **50**, 2755

Received 3rd December 2013,
Accepted 20th January 2014

DOI: 10.1039/c3cc49182j

www.rsc.org/chemcomm

Zhao Zhao,[ab] Huaqiao Tan,*[a] Haifeng Zhao,[a] Yang Lv,[c] Li-Jing Zhou,[d] Yujiang Song[c] and Zaicheng Sun*[a]

Stable reduced TiO_2 rutile nanorods with well-defined facets were prepared by a solvothermal route in the presence of Zn powder. The oxygen vacancy in the TiO_2 nanorods, which can be tuned by the amount of Zn, results in a narrow band gap and visible-light photocatalytic activity.

Titanium dioxide (TiO_2) has been extensively employed in many solar energy conversion applications such as photovoltaics, photocatalytic organic waste degradation, and water splitting for H_2 production and is known to be a promising photocatalyst due to its good chemical, thermal and biological stability.[1] However, the large band gap of TiO_2 severely hinders its practical application because TiO_2 only absorbs UV light, which is lower than 5% of the full solar spectrum. Many efforts have been made to make TiO_2 with visible-light response. For example, doped TiO_2 with metal or non-metal ions exhibited a broad visible light absorption and great performance.[2] Recently, reduced TiO_2 (TiO_{2-x}), incorporating Ti^{3+} and/or oxygen vacancies in TiO_2, has emerged as an effective route to obtain visible-light photoactivity.[3] However, theoretical work has suggested that, in order to achieve an efficient activity in the visible spectrum, the concentration of Ti^{3+} must be sufficiently high to induce a continuous vacancy band of electronic states just below the conduction band edge of TiO_2.[4] Otherwise, a low Ti^{3+} doping concentration only creates localized oxygen vacancy states that deteriorate the electron mobility which results in a negligible visible photo activity. This is due to the fact that the energy of the scattered doping states is largely (0.75–1.18 eV) below the conduction band edge of TiO_2 and the occupying photo-electrons are not adequately reactive and/or mobile for desired electrochemical reactions.[5–7] Therefore, doping with a high concentration of Ti^{3+} in TiO_2 is essential to enhance the photocatalytic activity in the visible region.

Several techniques have been reported to produce TiO_{2-x} including thermal treatment under vacuum[8] or reducing conditions,[3b,9–11] electrons[12] or Ar^+ ion[13] bombardment, and hydrothermal treatment.[3d,f,14] Most reported procedures start from TiO_2, from which a fraction of the Ti^{4+} ions is reduced to Ti^{3+} under harsh reducing conditions such as high temperature in reducing gas (H_2 or CO). Furthermore, since the reduction occurs mainly on the surface of TiO_2, the oxygen vacancies are usually not stable enough, even in air. The TiO_{2-x} with surface oxygen vacancy (Ti^{3+}) could be easily oxidized to TiO_2 within a short period. Thus it is still a great challenge to develop a facile synthetic route to prepare stable reduced TiO_2 nanocrystals with well-defined facets.

In this report, we demonstrate a simple and facile solvothermal strategy for preparing highly active and stable TiO_{2-x} rutile nanorods with exposed (110) facets and tunable oxygen vacancy. The key step is that a $TiCl_3$ aqueous solution was employed as the starting material to make oxygen vacancies uniformly dispersed in the whole TiO_2 nanocrystal. Zn powder was added into the reaction to avoid the oxidation of Ti^{3+}, and tune the oxygen vacancy concentration and the crystalline phase. When the amount of Zn powder added is increased, the color of reduced TiO_2 nanocrystals gradually turns into dark blue and the crystals are in the rutile phase. That means reduced TiO_2 in the rutile phase is more stable. The blue TiO_{2-x} rutile nanorods can be stored at room temperature over a year without loss of activity. The photocatalytic performance of TiO_{2-x} reaches maximum when all the TiO_2 nanocrystals just turned into the rutile phase.

Typically, 1 mL of $TiCl_3$ (15–20%) aqueous solution was added into 30 mL isopropanol, and then Zn powder (0.5–2.5 mmol) was added into the above solution. After stirring for about 30 min, the solution mixture was transferred into a dried Teflon autoclave container. Then the reaction was placed into an oven at 180 °C for 6 hours. The obtained solid was collected and washed with 100 mL of 4 mol L^{-1} HCl aqueous solution over 12 hours to remove excess Zn powder. After that, the solid was washed with distilled water 3 times, and then dried at 70 °C. EDAX results (Fig. S1, ESI†)

[a] *State Key Laboratory of Luminescence and Applications, Changchun Institute of Optics, Fine Mechanics and Physics, Chinese Academy of Sciences (CAS), Changchun, Jilin 130033, China. E-mail: tanhq870@126.com, sunzc@ciomp.ac.cn*
[b] *University of Chinese Academy of Sciences, Beijing 100000, China*
[c] *Dalian National Laboratories for Clean Energy, Dalian Institute of Chemical Physics, CAS, Dalian, Liaoning 116023, China*
[d] *State Key Laboratory of Inorganic Synthesis and Preparation, Jilin University, Changchun, Jilin 130012, China*

† Electronic supplementary information (ESI) available: Detailed experiments and characterization, XRD, SEM, and N_2 adsorption. See DOI: 10.1039/c3cc49182j

indicate that no Zn signal is observed. This reveals that the Zn has been totally removed by the acid washing step.

When the $TiCl_3$ aqueous solution was added into water, the color of the solution turned from blue purple into transparent within a short period, indicating that the Ti^{3+} is easily oxidized to Ti^{4+}. Only white anatase TiO_2 nanocrystals are obtained after the hydrothermal reaction (Fig. S2, ESI†). Isopropanol is chosen as the solvent instead of water because Ti^{3+} can survive in the isopropanol solution. After the solvothermal reaction, gray TiO_2 nanocrystals were obtained. X-ray diffraction (XRD) patterns (Fig. S3, ESI†) indicate that the obtained TiO_2 is a mixture of anatase and rutile TiO_2, indicating that most of the Ti^{3+} is oxidized and forms TiO_2 in the solvothermal reaction. To avoid the oxidation of Ti^{3+}, Zn powder is added into the solvothermal reaction. The as-prepared TiO_2 nanocrystals show a series color change from gray to dark blue upon the addition of different amounts of Zn (Fig. 1C, insets). The UV-Vis spectra of reduced TiO_2 nanocrystals, as shown in Fig. 1A, disclose that a broad absorption band appears in the visible region and it turns stronger upon the addition of different amounts of Zn powder. When the amount of Zn powder is increased to 1.5 mmol, the optical band gap of reduced TiO_2 changes to 2.93 eV (Fig. S4, ESI†). Fig. 1B shows the XRD patterns of the reduced TiO_2 nanocrystal samples. The relative amount of rutile phase in the reduced TiO_2 gradually increases with increasing amounts of Zn powder. When 1.5 mmol of Zn powder was added into the reaction, only rutile TiO_2 nanocrystals were obtained. Although Huang *et al.* obtained the Ti^{3+} self-doped TiO_2 through the hydrothermal route with Zn powder and Ti^{4+}, Zn^{2+} was detected at the surface of TiO_2 nanocrystals.[3f] In our case, no Zn signal is observed in the EDAX (Fig. S1, ESI†) and X-ray photoelectron spectroscopy XPS full scan spectra (Fig. S5, ESI†). High resolution XPS of Ti 2p, as shown in Fig. 1C, reveals that the peaks at 458.3 and 464.1 eV, attributed to Ti $2p_{3/2}$ and Ti $2p_{1/2}$, shift to low binding energies of 457.8 and 463.5 eV, respectively. This shift indicates that the Ti^{3+} doped TiO_2 is formed and the oxygen vacancy concentration increases in the TiO_2 nanocrystals with the increase of the amount of Zn powder. Electron paramagnetic resonance (EPR) spectroscopy was employed to determine the presence of Ti^{3+}. A strong EPR signal is observed at $g = 1.96$ (Fig. 1D), which could be assigned to Ti^{3+},[15] thus confirming the existence of the Ti^{3+} in the nanorods. No EPR signal at $g = 2.02$ implies that all of the Ti^{3+} located in the bulk, which is crucial for the stability of our reduced TiO_2 nanorods.[3d]

Fig. 2 shows transmission electron microscopy (TEM) images of the reduced TiO_2 nanocrystals prepared by the solvothermal reaction with different amounts of Zn powder. When the amount of Zn powder is lower than 0.5 mmol, the TiO_2 nanocrystals are mainly in the anatase phase and in truncated octahedron (Fig. 2A). The high resolution TEM image (inset) also shows clear 0.35 nm lattice fringes, corresponding to the (101) lattice plane of anatase TiO_2. When the amount of Zn powder is increased to 1.0 mmol, there are two TiO_2 morphologies observed, truncated octahedron anatase TiO_2 and rutile TiO_2 nanorods with exposed (110) facets. Upon further increasing the amount of Zn powder to 1.5 mmol, only the rutile TiO_2 nanorods with 50 nm length and ~5 nm diameter were obtained. High-resolution TEM images reveal 0.32 nm lattice fringes, corresponding to the (110) lattice plane of rutile TiO_2. Upon further increasing the amount of Zn powder, the TiO_2 morphology (Fig. 2D) shows no obvious change. These TEM results indicate that all TiO_2 nanocrystals possess well-defined facets, for example, TiO_2 rutile nanorods with exposed (110) facets. Small aggregation composed with a few TiO_2 nanorods can be observed in the SEM images (Fig. S6, ESI†). The N_2 absorption was employed to evaluate the surface area of obtained TiO_2 nanocrystals. Fig. S7 (ESI†) shows the

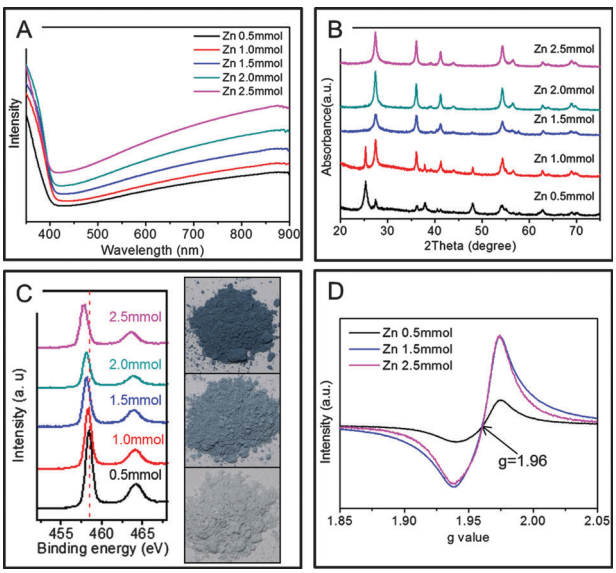

Fig. 1 The characterization of reduced TiO_2 prepared by a solvothermal reaction with different amounts of Zn powder (line color black, red, blue, cyan, and purple for 0.5, 1.0, 1.5, 2.0, and 2.5 mmol, respectively). (A) UV-visible absorbance spectra (converted from diffuse reflectance spectra), (B) XRD patterns, (C) high resolution Ti 2p XPS spectra, insets are optical images of reduced TiO_2 obtained from 2.5, 1.5 and 0.5 mmol of Zn powder from top to bottom. (D) EPR spectra.

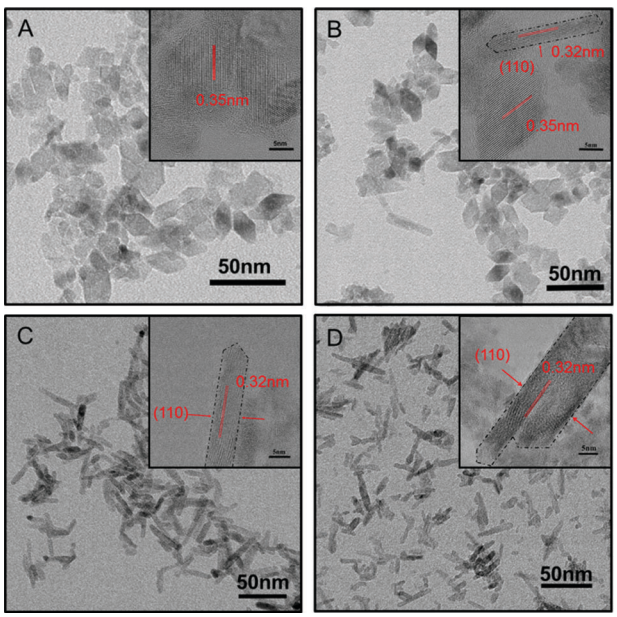

Fig. 2 TEM images of reduced TiO_2 prepared by a solvothermal reaction in the presence of 0.5, 1.0, 1.5 and 2.5 mmol of Zn powder. Insets are the corresponding high-resolution TEM images.

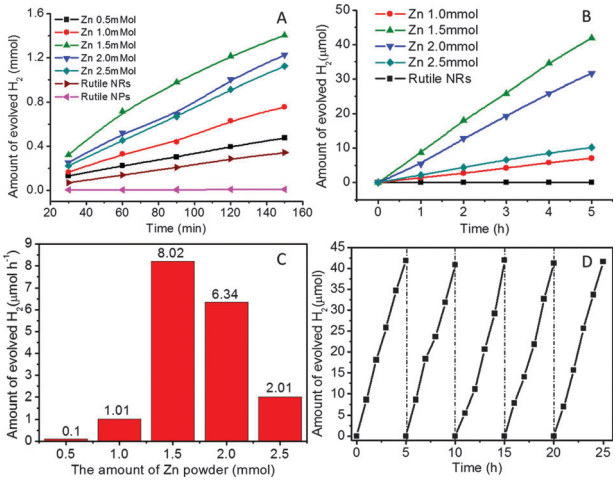

Fig. 3 Time courses of H_2 production from reduced TiO_2 loaded with 0.5% Pt in 20% methanol–water under irradiation of a xenon lamp (300 W) without (A) and with (B) UV-420 cut-off filter illumination. (C) H_2 production rate for reduced TiO_2 prepared from different amounts of Zn powder under visible light ($\lambda > 420$ nm). (D) Cycling tests of photocatalytic activity of reduced TiO_2 prepared from 1.5 mmol Zn powder under visible light ($\lambda > 420$ nm). Rutile NPs is TiO_2 nanoparticles ~30 nm in diameter. Rutile NRs were prepared from reduced TiO_2 calcined at 450 °C for 30 min.

N_2 absorption curves, which exhibit typical type IV curves. The BET surface area of TiO_2 nanocrystals gradually decreases from 90 $m^2\ g^{-1}$ to 55 $m^2\ g^{-1}$ from anatase TiO_2 truncated octahedron to rutile nanorods, respectively.

Photocatalytic water splitting H_2 production was used to evaluate the photocatalytic activity of as-obtained TiO_{2-x} nanocrystals. Fig. 3A shows a typical time course of H_2 evolution in the full solar spectrum (xenon lamp 300 W). Normal rutile nanoparticles (~30 nm in diameter purchased from Aladdin Reagent. Inc.) show very weak photocatalytic activity. Rutile TiO_2 nanorods prepared from reduced TiO_2 nanorods calcined at 450 °C for 30 min show ~0.14 mmol h^{-1} per 0.1 g photocatalyst. For the reduced TiO_2, the H_2 evolution amount at the same time period increases with the increase of the rutile ratio in the mixture of reduced TiO_2 nanocrystals. The H_2 production amount reaches the maximum ~0.6 mmol per hour for 0.1 g reduced TiO_2 when reduced TiO_2 completely transfer into the rutile phase. After that, the H_2 evolution amount decreases, indicating that the photocatalytic performance decreases in the case of very high oxygen vacancy concentration, which is caused by the over-reduction of excess amount of Zn powder. The H_2 evolution curve, under visible light ($\lambda > 420$ nm, a xenon lamp with a 420 nm cut-off filter), is shown in Fig. 3B. The reduced TiO_2 rutile nanorods show a stable H_2 release rate of ~8 μmol per hour per 0.1 g photocatalyst. The normal Rutile TiO_2 nanoparticles and TiO_2 nanorods with defined facets show no H_2 production under visible light ($\lambda > 420$ nm). The probable mechanism is that the oxygen vacancies narrow the band gap of TiO_2 and promote the charge separation of photo generated charge carriers (Fig. S9, ESI†). The photocatalytic activity is still maintained without a noticeable decrease after recycling five times (Fig. 3D), demonstrating the excellent stability of the reduced TiO_2.

In conclusion, we have developed a simple one-step method to synthesize reduced TiO_2 rutile nanorods with well-defined facets. The as-prepared reduced TiO_2 exhibits high stability in air and water upon light irradiation. The reduced degree (oxygen vacancy concentration) can be tuned by the amount of Zn powder added. Experimental results show a good conversion efficiency in both the full solar spectrum and visible light ($\lambda > 420$ nm), which supports that it is the introduced oxygen vacancy that accounts for the extension of the photocatalytic activity from the UV to the visible light region. Excess amount of oxygen vacancy will result in a decrease of photocatalytic performance. The present study demonstrates a simple and economical method for narrowing the band gap and for the development of a highly active photocatalyst under visible light.

We acknowledge the financial support from the National Natural Science Foundation of China (No. 21201159, 61176016, and 21104075), the Science and Technology Department of Jilin Province (No. 20121801), ''Hundred Talent Program'' CAS and open research fund of Key Laboratory of Functional Inorganic Material Chemistry (Heilongjiang University).

Notes and references

1 (*a*) M. Graetzel, R. A. J. Janssen, D. B. Mitzi and E. H. Sargent, *Nature*, 2012, **488**, 304–312; (*b*) A. Hagfeldt, G. Boschloo, L. Sun, L. Kloo and H. Pettersson, *Chem. Rev.*, 2010, **110**, 6595–6663; (*c*) X. Chen, S. Shen, L. Guo and S. S. Mao, *Chem. Rev.*, 2010, **110**, 6503–6570; (*d*) A. L. Linsebigler, G. Lu and J. T. Yates, *Chem. Rev.*, 1995, **95**, 735–758; (*e*) H. Chen, C. E. Nanayakkara and V. H. Grassian, *Chem. Rev.*, 2012, **112**, 5919–5948; (*f*) J. Su, X. Zou, G. D. Li, Y. M. Jiang, Y. Cao, J. Zhao and J. S. Chen, *Chem. Commun.*, 2013, **49**, 8217–8219.
2 (*a*) M. Anpo, *Pure Appl. Chem.*, 2000, **72**, 1787–1792; (*b*) A. Fuerte, M. D. Hernandez-Alonso, A. J. Maira, A. Martinez-Arias, M. Fernandez-Garcia, J. C. Conesa and J. Soria, *Chem. Commun.*, 2001, 2718–2719; (*c*) B. Liu, H. M. Chen, C. Liu, S. C. Andrews, C. Hahn and P. Yang, *J. Am. Chem. Soc.*, 2013, **135**, 9995–9998; (*d*) J. Cao, Y. Zhang, L. Liu and J. Ye, *Chem. Commun.*, 2013, **49**, 3440–3442; (*e*) R. Asahi, T. Morikawa, T. Ohwaki, K. Aoki and Y. Taga, *Science*, 2001, **293**, 269–271; (*f*) F. Dong, S. Guo, H. Wang, X. Li and Z. Wu, *J. Phys. Chem. C*, 2011, **115**, 13285–13292; (*g*) S. In, A. Orlov, R. Berg, F. García, S. Pedrosa-Jimenez, M. S. Tikhov, D. S. Wright and R. M. Lambert, *J. Am. Chem. Soc.*, 2007, **129**, 13790–13791; (*h*) G. Liu, Y. Zhao, C. Sun, F. Li, G. Q. Lu and H.-M. Cheng, *Angew. Chem., Int. Ed.*, 2008, **47**, 4516–4520; (*i*) S. G. Kumar and L. G. Devi, *J. Phys. Chem. A*, 2011, **115**, 13211–13241.
3 (*a*) I. Justicia, P. Ordejón, G. Canto, J. L. Mozos, J. Fraxedas, G. A. Battiston, R. Gerbasi and A. Figueras, *Adv. Mater.*, 2002, **14**, 1399–1402; (*b*) F. Zuo, L. Wang, T. Wu, Z. Zhang, D. Borchardt and P. Feng, *J. Am. Chem. Soc.*, 2010, **132**, 11856–11857; (*c*) X. Chen, L. Liu, P. Y. Yu and S. S. Mao, *Science*, 2011, **331**, 746–750; (*d*) F. Zuo, K. Bozhilov, R. J. Dillon, L. Wang, P. Smith, X. Zhao, C. Bardeen and P. Feng, *Angew. Chem., Int. Ed.*, 2012, **51**, 6223–6226; (*e*) Z. Zheng, B. Huang, J. Lu, Z. Wang, X. Qin, X. Zhang, Y. Dai and M.-H. Whangbo, *Chem. Commun.*, 2012, **48**, 5733; (*f*) Z. Zheng, B. Huang, X. Meng, J. Wang, S. Wang, Z. Lou, Z. Wang, X. Qin, X. Zhang and Y. Dai, *Chem. Commun.*, 2013, **49**, 868–870; (*g*) J. Su, X. Zou, Y. Zou, G. D. Li, P. P. Wang and J. S. Chen, *Inorg. Chem.*, 2013, **52**, 5924–5930.
4 D. C. Cronemeyer, *Phys. Rev.*, 1959, **113**, 1222–1226.
5 J. Nowotny, T. Bak, M. K. Nowotny and L. R. Sheppard, *J. Phys. Chem. B*, 2006, **110**, 18492–18495.
6 M. K. Nowotny, L. R. Sheppard, T. Bak and J. Nowotny, *J. Phys. Chem. C*, 2008, **112**, 5275–5300.
7 V. N. Kuznetsov and N. Serpone, *J. Phys. Chem. C*, 2009, **113**, 15110–15123.
8 V. E. Henrich and R. L. Kurtz, *Phys. Rev. B*, 1981, **23**, 6280–6287.
9 H. Liu, H. T. Ma, X. Z. Li, W. Z. Li, M. Wu and X. H. Bao, *Chemosphere*, 2003, **50**, 39–46.
10 Y. Li, X. Li, J. Li and J. Yin, *Mater. Lett.*, 2005, **59**, 2659–2663.
11 G. Wang, H. Wang, Y. Ling, Y. Tang, X. Yang, R. C. Fitzmorris, C. Wang, J. Z. Zhang and Y. Li, *Nano Lett.*, 2011, **11**, 3026–3033.
12 G. A. Kimmel and N. G. Petrik, *Phys. Rev. Lett.*, 2008, **100**, 196102.
13 S. Hashimoto and A. Tanaka, *Surf. Interface Anal.*, 2002, **34**, 262–265.
14 X. Liu, S. Gao, H. Xu, Z. Lou, W. Wang, B. Huang and Y. Dai, *Nanoscale*, 2013, **5**, 1870–1875.
15 J. C. Conesa and J. Soria, *J. Phys. Chem.*, 1982, **86**, 1392–1395.